

The Role of Impingement Angle and Velocity on the Solid Particle Erosion Behavior of Agave Lechuguilla Fiber-Reinforced Polymer Composite

Sudhakar Majhi¹  · Subhrajit Pradhan¹ · Ved Prakash¹ · S. K. Acharya¹

Received: 20 March 2023 / Accepted: 15 May 2023 / Published online: 9 June 2023
© The Indian Institute of Metals - IIM 2023

Abstract In this research, short Agave lechuguilla (AL) fibers were used as reinforcement material in epoxy resin at different weight percentages (10, 20, 30, and 40 wt.%) to make a composite by hand lay-up techniques. The rate of erosion and wear behavior of the fabricated composites against the varied impingement angles (30, 40, 60, and 90°) and different striking velocities (i.e., 48, 70, 80, and 109 m/s) of erodent have been studied using an erosion test rig. It was observed that by adding the short AL fibers in epoxy resin, the resistance to wear of pure epoxy decreases, and the mode of failure also changes. The wear rate of composites was maximum at 45° impingement angle and at lower impact velocities (i.e., 48 m/s and 70 m/s), representing the mode of erosion is semi-ductile. However, at higher impingement angles (60°) and impact velocities (80 m/s and 109 m/s), the mechanism of erosion was semi-brittle. Scanning electron microscope (SEM) analysis was carried out to study the morphology of eroded surfaces.

Keywords Agave lechuguilla fiber · Wear rate · Erosion · SEM · Mode of erosion

1 Introduction

The community of material designers and researchers seems to have reached a consensus in recent times to choose natural fibers as an alternative to synthetic ones as an option for use in polymer composites due to the prevalent ecological,

geographical, and economic viewpoints. It has made it necessary to investigate the viability and effectiveness of various natural fibers in a variety of applications, which has necessitated the work of exploring diverse natural fibers. In this aspect, several researchers have put forward some regional natural fibers, such as Sisal [1], areca sheath [2], Luffa cylindrical [3], etc., as potential reinforcing materials and studied structural and tribological performances of the composites. Erosive wear is considered a widely experienced and critical tribological phenomenon for engineering materials, which affects the performance of components in various applications such as automobiles, aerospace structures, surface deterioration of steam turbine blades, erosion of sludge-transporting pipes, household articles (door and window) in desert areas, pump impeller blades along with green energy industries, etc. The important parameters that affect the erosive behavior of a material are represented in Fig. 1 [4].

Among the above-mentioned parameters, the impingement angle of erodent is one of the essential parameters, which describe the mode of erosive behavior. The mode of erosion is ductile if the maximum wear occurs at a lower impingement angle (15°–30°). Likewise, if the maximum erosion takes place at a high impact angle of 90°, the mode of erosion is brittle [5]. It is also mentioned by various researchers that the mode of erosion changes for unreinforced matrix when reinforced with fibers [3]. Abrasive, adhesive, and erosion failure modes are all common in many manufacturing sectors. Though the contribution of erosion wear is minor in comparison to other types of failure, its presence is found to be very serious in the mining and steel industries [6]. While working on different types of polymers for tribological applications, Friedrich [7] concluded that the inclusion of different types of fibers along with micro- and nano-fillers enhances the tribological behavior.

✉ Sudhakar Majhi
smnitrkl@gmail.com

¹ Department of Mechanical Engineering, National Institute of Technology Rourkela, Rourkela, India

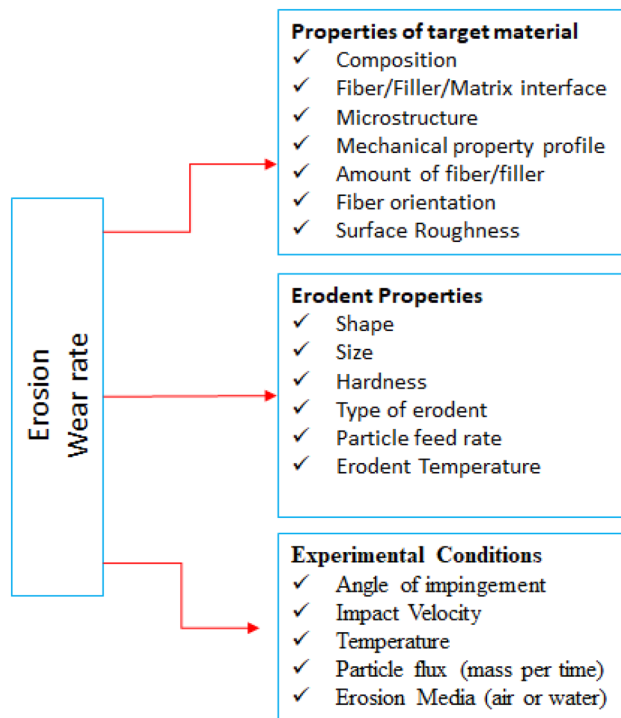


Fig. 1 Parameters affecting erosion wear rate

Gupta et al. [8] in their work reported that incorporating bidirectional bamboo fibers into epoxy resin enhances erosion resistance of neat epoxy. They also noticed that the highest erosion occurs at an angle of 60° – 75° , irrespective of the bamboo fiber weight percentage in the composite. By incorporating bamboo fiber, the semi-ductile behavior of neat epoxy changes to semi-brittle.

Prakash et al. [9] analyzed the erosive wear behavior of the composites reinforced with short *Syngonanthus nitens* natural fiber. They observed that when the fiber reinforcement is limited to 20 wt.%, the wear resistance increases; beyond that, the wear resistance diminishes. They also came to the conclusion that most erosion happens at lower velocities (48 m/s and 70 m/s) with an impingement angle of 45° . When the impinging erodent's velocity increases to 80 m/s and 109 m/s, the maximum erosion appears to occur at an impingement angle of 60° . As a result, the mode of erosion shifts from semi-ductile to semi-brittle.

Pradhan et al. [10] studied the significance of *Eulaliopsis binata* fiber reinforcement on the erosive behavior of neat epoxy. They found that the inclusion of EB fiber up to 30 wt.% boosts resistance to erosion of the neat epoxy; beyond that, resistance to erosion decreases. They also claimed that the peak erosion took place at an impingement angle of 45° when the velocity of erodent was 48 m/s and 70 m/s. As the impingement velocity enhanced to 82 m/s and 109 m/s, the highest erosion occurred at a 60°

impingement angle, which represents the mode of erosion shifts from semi-ductile to semi-brittle.

Deo et al. [11] fabricated composites with short *Lantana-camara* fiber by hand lay-up techniques, changing the weight percent of fiber from 0 to 40% in 10 wt.% steps. They found that the inclusion of this fiber decreases resistance to wear of all the composites in contrast to neat epoxy. They also stated that the highest amount of erosion takes place at an impingement angle of 45° for each velocity (48, 70, 80, and 109 m/s) of the erodent's impact, indicating that the mode of erosion is semi-ductile.

Nayak et al. [12] studied the solid particle erosion behavior of short areca sheath fiber reinforced polyvinyl alcohol (PVA) and found that the reinforcement of this fiber reduces the erosion resistances of all composites loaded with varied percentages of areca sheath fiber. They also stated that the peak erosion occurs at a 45° impact angle, indicating a semi-ductile mechanism of erosion.

According to the above studies, reinforcing natural fibers like bamboo, *Syngonanthus nitens*, and *Eulaliopsis binata* in neat resin increases the erosion resistance; however, the reinforcement of *Lantana camara* decreases the erosion resistance of neat resin. Though some natural fibers acknowledge their utility as a reinforcement material in polymers for structural applications, it is essential to study their erosive behavior if they are to be used in an erosive environment.

Based on the review of the literature, it can be said that natural fiber plays a vital role in polymer composites for structural and tribological applications. Researchers have a significant challenge in the exploration of novel fibers, but it has to be appreciated with enormous effects on the composite industries.

Agave lechuguilla fiber is one such fiber whose potential as a reinforcing fiber has not been studied till now for its application in the area of tribology. The plant belongs to the Agavaceae family, which is often found in semi-arid and dry regions of Mexico and its neighboring regions. Because of its high tensile strength, low cost, low density, and environmental friendliness, fiber has been utilized in traditional applications such as ropes, utility items, brushes, and so on. Some researchers have utilized this fiber as a reinforcement material in polymers and cement concrete for structural applications [13]. In light of the aforementioned research gap, the current study is being conducted to analyze the erosive characteristic of AL fiber-reinforced epoxy composite. To examine the erosion characteristic of the developed composite, experimental parameters like varying impact velocities and impingement angles of the erodent particles have been taken into consideration. The energy-dispersive X-ray spectroscopy (EDX), X-ray diffraction (XRD), and scanning electron microscope (SEM) analysis have been carried out to characterize the fiber.

2 Experimental Details

2.1 Materials

The matrix material epoxy (Grade L12) and the curing agent (K6) were supplied by Lapox India limited. The AL fibers were provided by Galaxy Enterprises, Mumbai, and were imported from Mexico. The given material had a length of 25 mm and a diameter of 3.24 mm 4.53 mm. The fibers were cleansed thoroughly in normal water and then sun-dried for 4–5 days before being placed in an oven for 72 h to eliminate the moisture. The fibers were then cut to 9.8 mm and kept in a desiccator for future usage. This fiber length is the critical fiber length that was found by following the procedure from the fiber pull-out test [14]. The image of the Agave lechuguilla plant and its fiber is shown in Fig. 2.

2.2 Characterization Studies of AL Fiber

2.2.1 Energy-Dispersive Spectrometer Analysis

To determine the existing constituents that are present on the AL fiber surface, EDS analysis was performed using a spectrometer (Make: Oxford Instruments).

2.2.2 X-ray Diffraction Analysis

The X-ray spectra of AL fibers were obtained by X-ray diffractometer (Make and Model: RIGAKU, JAPAN & ULTIMA -IV). The range of the scan was taken as $2\theta = 5^\circ - 70^\circ$, where θ = angle of diffraction, speed of scanning 5.00 deg/min. The estimation of crystallinity indices was done from the peak of the intensity spectrum.

2.3 Fabrication of Composite

To fabricate the composite, the hand lay-up technique was adopted. A wooden mold with dimensions of $200 \times 60 \times 4 \text{ mm}^3$ was first prepared and fixed on a Perspex sheet that was placed on a flat smooth surface, followed by the application of mold-releasing silicon spray. Epoxy and hardener in precise proportions (10:1 ratio) were stirred in a container, then short AL fibers (having a critical length of 9.86 mm) were added to the mixture as per the rule of mixture and

mixed properly. Then, the prepared materials were poured into the mold and uniformly distributed. Then, heated air was blown on the top surface using a heat gun to remove the air bubbles entrapped. After that, a silicon-sprayed Perspex sheet was placed on the top, ensuring no air bubbles present inside the complete material. Then, a flat, smooth metal plate with dead weight was put on top of the mold and left to cure for 24 h. Following the above procedure, composites were fabricated with different weight percentages of AL fiber (i.e., 10, 20, 30, and 40 wt.%), which correspond to fiber volume fractions of 0.162, 0.329, 0.501, and 0.674, respectively. Then, the samples of sizes $24 \times 24 \times 4 \text{ mm}^3$ were prepared from these composites for erosion test.

2.4 Void Percentage of Composites

The void percentage of the composites made with different amounts of AL fibers (10, 20, 30, and 40 wt.%) were calculated, and the composites with a reasonable void percentage ($\leq 2\%$) were chosen for erosion test using the instructions provided by Prakash et al. [15]

2.5 Erosion Testing of Polymer Composite

To investigate the erosive wear characteristics of an epoxy composite reinforced with AL fibers at ambient temperature, an air jet erosion test rig (designed as per ASTM standard G76 and supplied by Magnum Engineers, Bangalore, India) was used, whose photographic view is shown in Fig. 3. The machine consists of an air compressor, pressure regulator, mixing chamber for air and erodent, nozzle, hopper, etc. From the hopper, the stored erodent particles are allowed to fall on the conveyer belt with a constant predetermined fixed rate (3gm/min). Then, the eroding particles are transported by a conveyor belt into a mixing chamber, where they are mixed with air at the right pressure. The mixture is then passed through the nozzle of diameter 4 mm and allowed to hit the samples fixed on the sample holder. The sample holder can hold the samples at varied angles with reference to striking particles. The velocity at which the erodent particles hit the sample surface is calculated by converting the air pressure to velocity using the double disc method [16]. The samples of sizes $24 \times 24 \times 4 \text{ mm}^3$ were used for the experiment. Different parameters

Fig. 2 a Agave lechuguilla plant b Agave lechuguilla long fiber c Agave lechuguilla short fiber



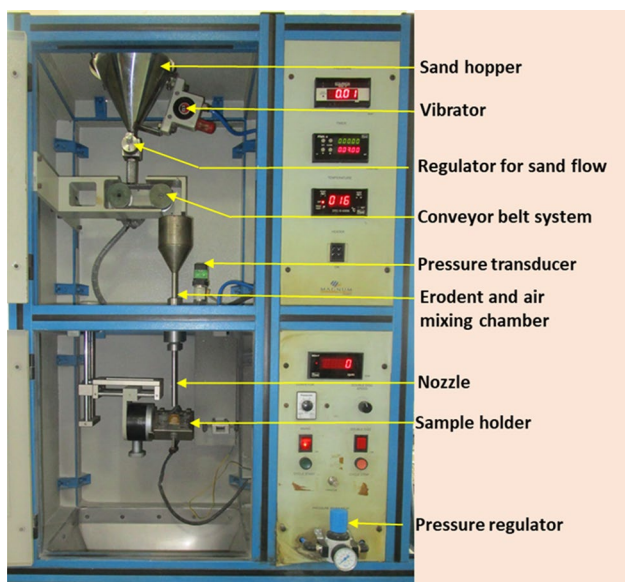


Fig. 3 Erosion testing machine

with which the erosion test was performed are compiled in Table 1. The specimens were thoroughly cleaned with acetone and weighed before and after the erosion test with an accuracy of ± 0.001 mg.

After each test, the erosion rate was estimated by applying the following formula.

$$E_r = \frac{\Delta w}{w_e} \tag{1}$$

where Δw represents the loss of mass of the eroded sample. w_e is the erodent particle mass (test time x feed rate). The test time was fixed for all the samples, i.e., 15 min.

Table 1 Erosion test parameters

Types of erodent	Silica particle
Structure of erodent	Irregular
Size of erodent (in microns)	200 ± 50
Silica particle hardness value (HV.)	1420 ± 50
Erodent’s impingement angle (θ°)	30, 45, 60, 90
Feed rate of erodent (gm/min)	3 ± 0.1
Striking velocity of erodent (m/s)	48, 70, 82, 109
Distance between nozzle and sample in mm (stand-off distance)	10

3 Experimental Results and Analysis

3.1 Characterization Studies of AL Fiber

The EDS spectra of AL fiber are displayed in Fig. 4, and Table 2 summarizes the numerous elements that can be identified in AL fiber. Figure 5a–f illustrates the EDS mapping of the essential components of the reference fiber. These components include carbon, oxygen, calcium, and silicon, and the mapping demonstrates that these atoms are equally distributed across the fiber surface. The evenly spread carbon, oxygen, calcium, and silicon atoms give the fiber more mechanical strength. The material is lighter and more robust because of the higher carbon content. The higher carbon content of fiber gives a lighter weight to the composite.

Figure 6 represents the XRD spectra of AL fiber. From the spectra, the peaks have been identified and calculated the crystallinity index as per the given formula. [17]

$$CI = \frac{I_{02} - I_{am}}{I_{02}} \times 100 \tag{2}$$

where CI = crystallinity index, I_{02} = crystallographic plane intensity, and I_{am} = amorphous plane intensity. The crystallinity index and % of crystallinity of the fiber have been found to be 43.85 and 64.04, respectively.

3.2 Behavior of Composite Under Erosion

As recommended by Pradhan. et al. [10] and Mohanta. et al. [3], the emphasis of this work has been on the role of varied impingement angle and impact velocity in determining the wear behavior of the composite, as stated below.

Figure 8a–d illustrates the erosion wear rate of the composites (reinforced with 0–40 wt.% of AL fiber in a step of 10 wt.%) with respect to different impingement angles (30, 45, 60, and 90°) for varied impingement velocities (48, 70, 82, and 109 m/s) of the erodent. In all these cases, it

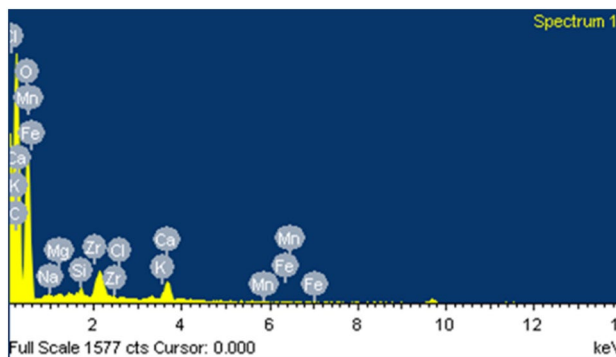


Fig. 4 EDS Spectra of AL fiber

Table 2 Elements present in AL fiber

Chemical Elements (Atomic %)	C	O	Ca	Si	Mg	K	Zr	Fe	Cl	Na	Mn
AL fiber	58.03	40.52	0.81	0.21	0.13	0.12	0.07	0.04	0.04	0.03	0.01

Fig. 5 EDS mapping of AL fiber surface representing **a** reference surface of fiber, **b** combination of all the elements, **c** carbon, **d** oxygen, **e** calcium, and **f** silicon

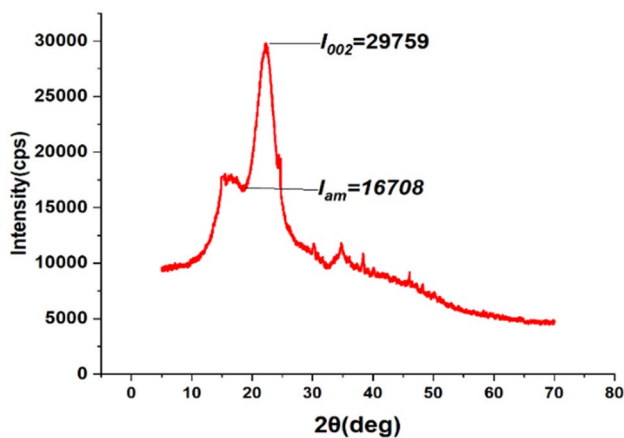
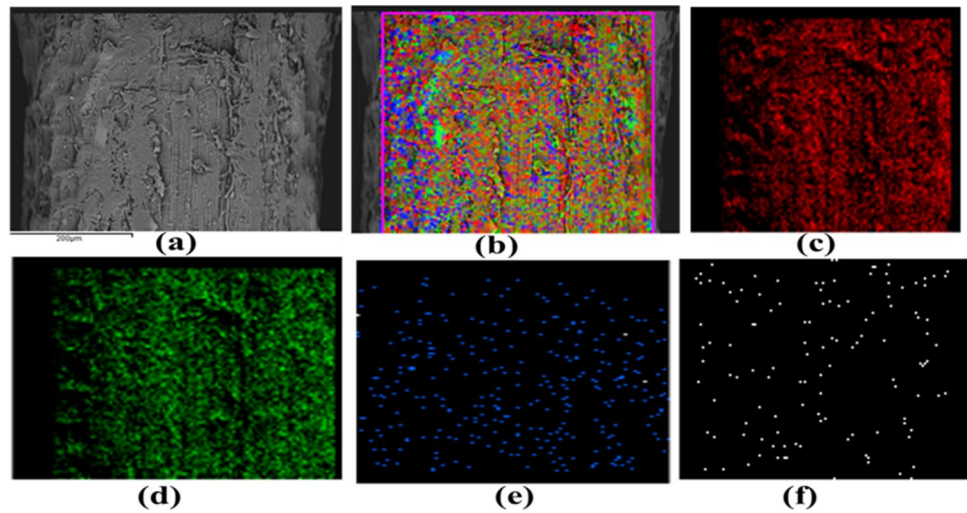


Fig. 6 XRD spectra of AL fiber

is observed that the erosion rate of neat epoxy is increasing with the addition of AL fibers. It is also observed that irrespective of impingement angle and impact velocity, the erosion wear rate of neat epoxy is minimum, and the erosion rate of the composite containing 40wt.% of AL fiber is maximum. At lower velocity impact of erodent (i.e., 48 m/s and 70 m/s), the maximum erosion occurs at 45° impingement angle for all the composites along with neat epoxy as shown in Fig. 8 (a, b). This could be due to a cutting mechanism of erodent by the $V \cos\theta$ component of velocity, which is the dominating factor (Fig. 7). When the erodent strikes the specimen at an impingement angle θ with a velocity of V m/s, the impacting velocity is divided into two components, i.e., $V \cos\theta$ and $V \sin\theta$, as

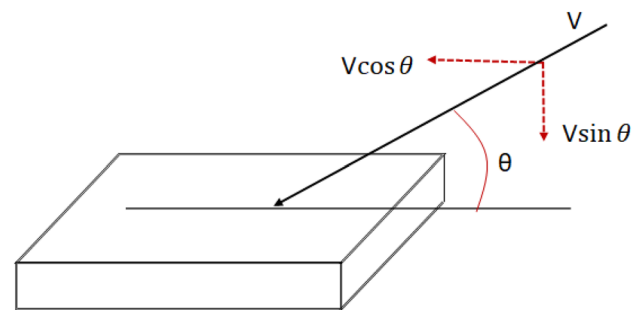


Fig. 7 Erodent striking the specimen

represented in Fig. 7. The $V \sin\theta$ component is perpendicular to the sample, whereas the $V \cos\theta$ component is parallel to the sample and is responsible for the cutting mechanism during erosion. The experimental result shows that at a lower velocity (48 m/s and 70 m/s), maximum erosion occurs at an angle of 45° for all the composites along with neat epoxy, which indicates that the nature of erosion is semi-ductile. Further, with increase in the velocity to 80 m/s, the maximum erosion angle shifts from 45° to 60°, indicating semi-brittle behavior for the composites as well as for the neat epoxy. Further, with increase in the velocity to 109 m/s, the erosion behavior of AL fiber composite remains the same (i.e., semi-brittle), whereas, at this velocity, the maximum erosion for pure epoxy occurs at 90°, which confirms its pure brittle behavior [9]. These modifications in erosive wear behavior are the result of the shearing activity of impacting particles at lower velocities. However, at higher velocities, the erosion rate

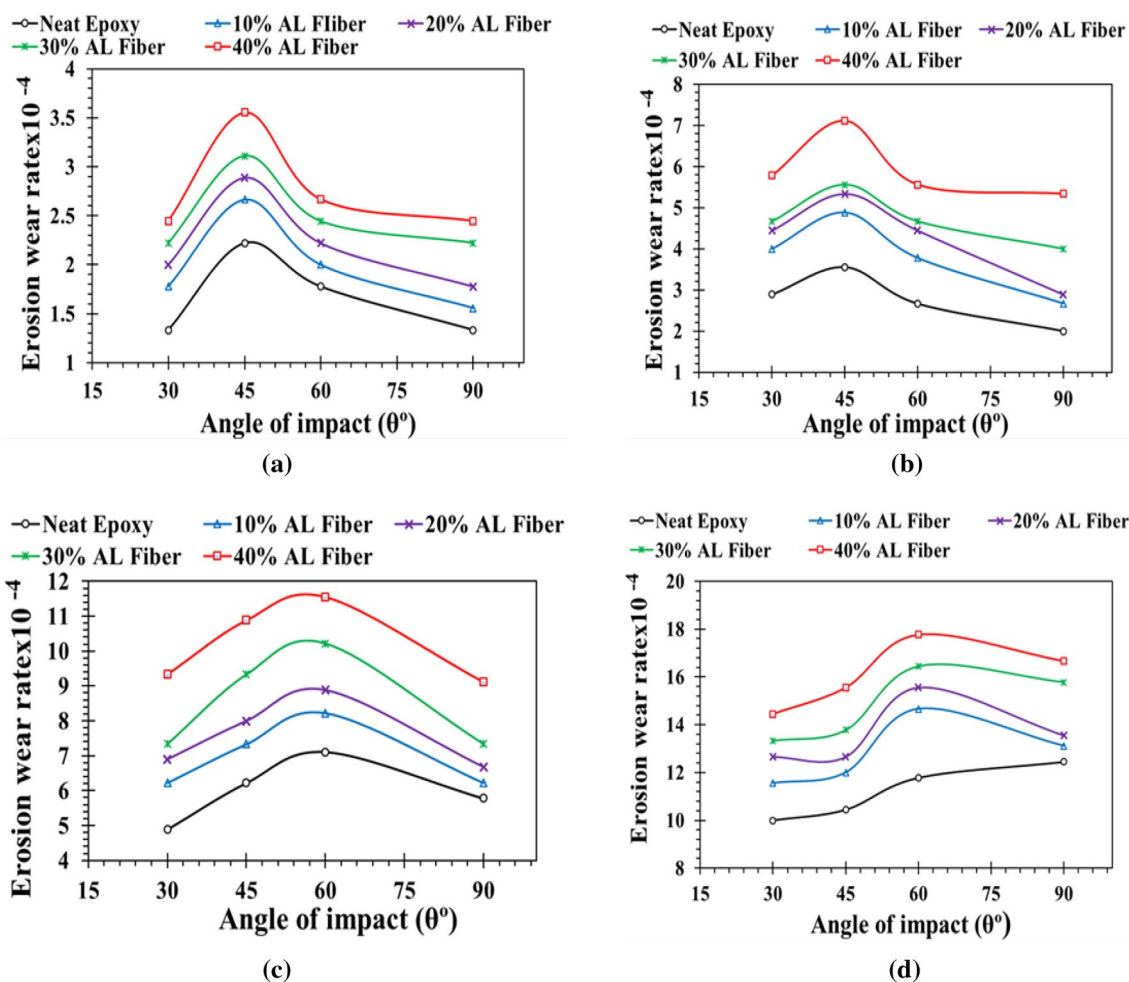


Fig. 8 Variation in rate of erosion w.r.t angle of impact and impact velocity **a** 48 m/s, **b** 70 m/s, **c** 80 m/s, and **d** 109 m/s

is dominated by impact forces caused due to the loss in kinetic energy of the erodent particles.

From the above study, it was found that the rate of erosion and its nature is not only dependent on the impingement angle but also depends upon the erodent impingement velocity. According to various researchers, when erosion rate (E_r) reaches its steady-state value, it can be represented as a power function of impact velocity (V) as $E_r = kV^n$, where k is the proportionality constant, and n = velocity exponent function. It has been established that if the value of n falls between 1 and 2, the erosion behavior is ductile, and if it falls between 4 and 6, the erosion behavior is brittle. Again, the erosion behavior is characterized as semi-ductile and semi-brittle if the value is between 2–3 and 3–4, respectively [9–11]. The values of k and n can be obtained by fitting the data points in the plots demonstrating the erosion rate dependency on impact velocity with a power law, as shown in Fig. 9a–d. The values of n for different composites and neat epoxy for varied impingement angles (30°, 45°, 60°, and 90°) are represented in Fig. 9a–d. From these plots, it is

found that the values of n lie between 1.23 and 2.2365. Thus, the velocity exponent function value indicates that erosion is semi-ductile in nature.

4 Morphology of Erosive Wear Surface

Figure 10a–h illustrates the eroded surface morphology of the composites containing AL fibers exposed to erodent at a higher velocity (109 m/s) with an impact angle of 60° during the erosion study.

Figure 10a, b displays microscopy of the eroded surface of a composite containing 10 wt.% AL fiber. The formation of craters, shearing of fiber and matrix, debonding of fiber and matrix interface, and micro-cracks are all clearly visible in the figure.

Figure 10c, d represents the SEM image of the eroded surface of the composite reinforced with 20 wt.% AL fiber. The figure shows that as the amount of fiber content increases, the failure of material due to erosion increases due

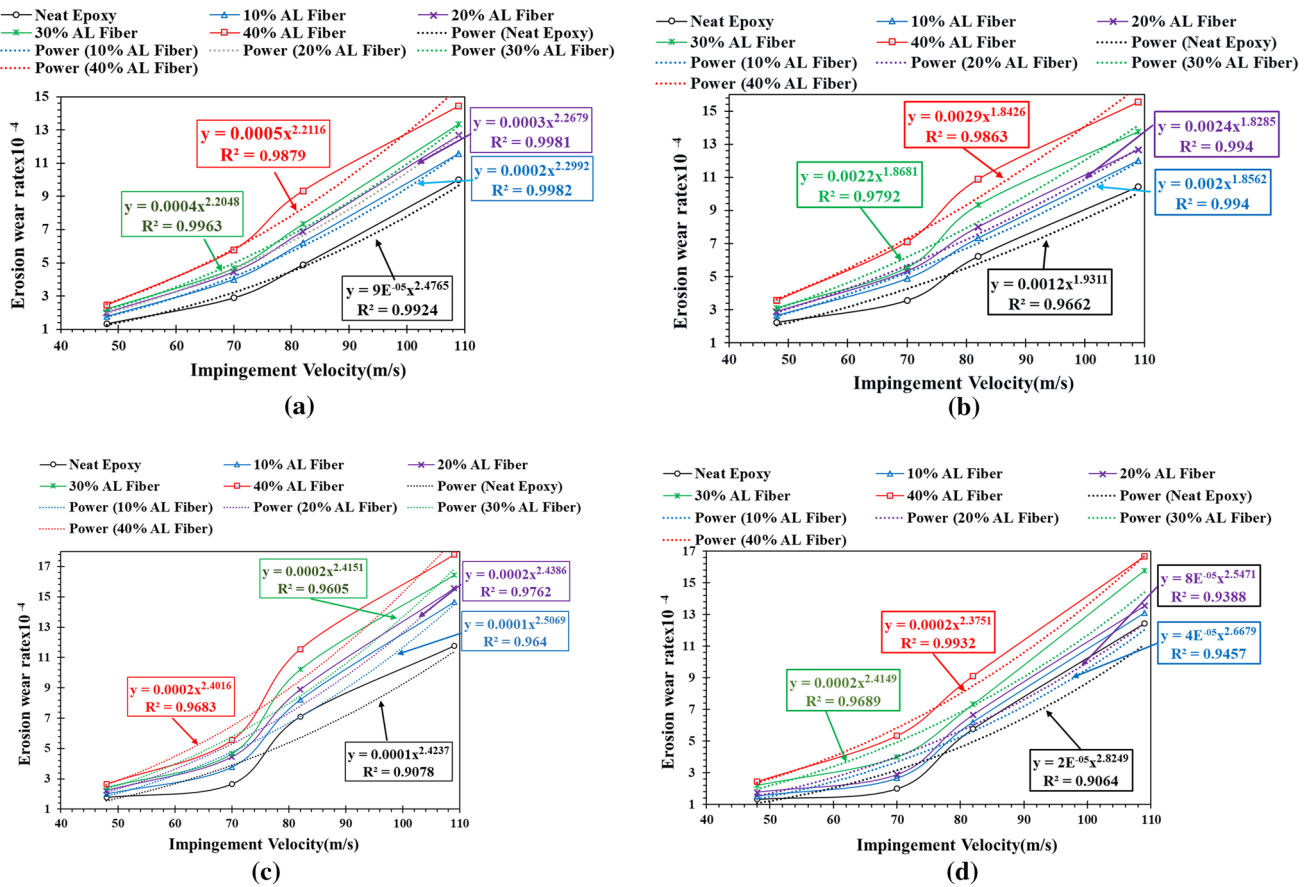


Fig. 9 Variation in rate of erosion w.r.t impingement velocity and impingement angle **a** 30°, **b** 45°, **c** 60°, and **d** 90°

to increased fragmentation of matrix material at the interface of fiber and matrix. The poor adhesion between fiber and matrix is incapable of sustaining the kinetic energy of high-speed impinging erodent, and hence failure initiates at the interface areas. In addition, craters and micro-cracks form near the weak interface zone. A similar type of material failure due to erosion is observed to a greater extent in composites containing 30 wt.% AL fiber, as represented in Fig. 10e, f.

The micrographs of Fig. 10g, h show the eroded surface of the composite containing 40wt.% of AL fiber. From the figure, it is observed that fiber debonding and fiber damage are becoming more prominent, and also fibers are coming out from the matrix. This could have happened because the increased amount of AL fiber has resulted in insufficient wetting of the fibers with the resin.

5 Conclusions

The short AL fiber epoxy composites were successfully fabricated, and the effect of fiber reinforcement, impingement velocity, and impact angle of erodent on the erosion behavior

of the fabricated composites was studied, leading to the following conclusions.

The angle and velocity of particle impact played a crucial role in determining the material failure mechanism owing to erosion.

A semi-ductile mode of erosion for all the AL fiber composites and neat epoxy was observed when the erodent struck the sample at lower speeds of 48 m/s and 70 m/s at an impingement angle of 45°.

As the velocity of the strike was increased to 80 m/s, the angle of impingement was shifted to 60° for maximum erosion of Al fiber composites and neat epoxy, indicating a semi-brittle mode of erosion.

When the velocity was increased further to 109 m/s, the erosion behavior of AL fiber composites remained unchanged (i.e., semi-brittle), whereas, at this velocity, the maximum erosion for pure epoxy occurred at a 90° impact angle, indicating pure brittle behavior.

The erosion rate of composites rises due to an increase in the percentage of fibers incorporated in the composite. The primary cause of the reduced erosion resistance was the poor adhesion between the AL fiber and epoxy matrix.

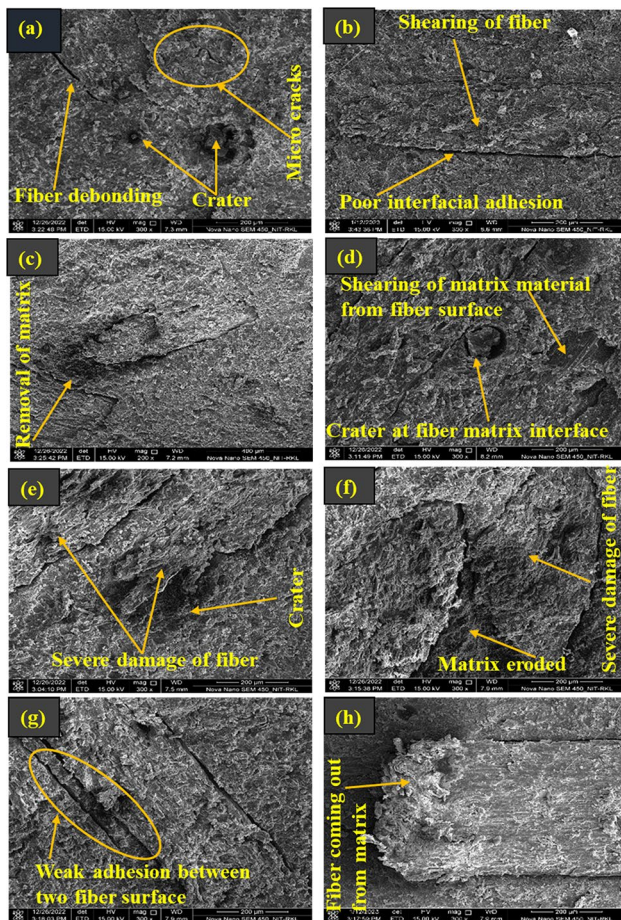


Fig. 10 SEM images of eroded surfaces at impingement angle 45° and impact velocity 70 m/s of the composites containing **a, b** 10% AL fiber **c, d** 20% AL fiber **e, f** 30% AL fiber **g, h** 40% AL fiber

Composites reinforced with 10% AL fiber provided higher erosion resistances than composites reinforced with 10, 20, and 30 wt.% AL fiber.

According to the SEM study of eroded surfaces, material failure was mostly caused by the formation of craters, micro-cracks, debonding of fiber, shearing of fiber and matrix, inadequate interfacial adhesion between fiber and matrix, etc.

References

- Sahu P, and Gupta M K, *Mater Res Express* **8** (2019) 085348. <https://doi.org/10.1088/2053-1591/ab29b5>
- Nayak S, and Mohanty J, *Communications* **18** (2020) 19. <https://doi.org/10.1016/j.coco.2020.01.006>
- Mohanta N, and Acharya S K, *BioResources* **10** (2015) 8364. <https://doi.org/10.15376/biores.10.4.8364-8377>
- Kaundal R, *Silicon* **9** (2017) 223. <https://doi.org/10.1007/s12633-014-9191-5>
- Cai F, Gao F, Pant S, Huang X, and Yang Q, *J Mater Eng Perform* **25** (2016) 290. <https://doi.org/10.1007/s11665-015-1848-8>
- Suresha B, Siddaramaiah K, Seetharamu S, and Kumaran P S, *Wear* **267** (2009) 1405. <https://doi.org/10.1016/j.wear.2009.01.026>
- Friedrich K, *Adv Ind Eng Polym Res* **1** (2018) 3. <https://doi.org/10.1016/j.aiepr.2018.05.001>
- Gupta A, Kumar A, Patnaik A, and Biswas S, *Int J Polym Sci* **2011** (2011) 12. <https://doi.org/10.1155/2011/592906>
- Prakash V, Pradhan S, and Acharya S K, *Trans Indian Inst Met* **74** (2021) 1741. <https://doi.org/10.1007/s12666-021-02268-9>
- Pradhan S, and Acharya S K, *Proc Inst Mech Eng Part J J Eng Tribol* **235** (2021) 830. <https://doi.org/10.1177/1350650120931645>
- Deo C, and Acharya S K, *Polym Plast Technol Eng* **48** (2009) 1084. <https://doi.org/10.1080/03602550903094340>
- Nayak J, and Mohanty S, *Compos Commun* **18** (2020) 19. <https://doi.org/10.1016/j.coco.2020.01.006>
- Juárez C, Guevara B, Valdez P, and Durán-Herrera A, *Constr Build Mater* **24** (2010) 1536. <https://doi.org/10.1016/j.conbuildmat.2010.02.007>
- Fiore V, Scalici T, Nicoletti F, Vitale G, Prestipino M, and Valenza A, *Compos Part B Eng* **85** (2016) 150. <https://doi.org/10.1016/j.compositesb.2015.09.028>
- Prakash V, Pradhan S, Majhi S, and Acharya S K, *Proc Inst Mech Eng Part L J Mater Des Appl* **237** (2022) 1. <https://doi.org/10.1177/14644207221123142>
- Ruff A W, and Ives L K, *Wear* **35** (1975) 195. [https://doi.org/10.1016/0043-1648\(75\)90154-4](https://doi.org/10.1016/0043-1648(75)90154-4)
- Segal L, Creely J J, Martin A E, and Conrad C M, *Text Res J* **29** (1959) 786. <https://doi.org/10.1177/004051755902901003>

Publisher's Note Springer Nature remains neutral with regard to jurisdictional claims in published maps and institutional affiliations.

Springer Nature or its licensor (e.g. a society or other partner) holds exclusive rights to this article under a publishing agreement with the author(s) or other rightsholder(s); author self-archiving of the accepted manuscript version of this article is solely governed by the terms of such publishing agreement and applicable law.